


Targeted metabolomics reveals differential biological effects of nanoplastics and nanoZnO in human lung cells

Swee Ling Lim, Cheng Teng Ng, Li Zou, Yonghai Lu, Jiaqing Chen, Boon Huat Bay, Han-Ming Shen & Choon Nam Ong

To cite this article: Swee Ling Lim, Cheng Teng Ng, Li Zou, Yonghai Lu, Jiaqing Chen, Boon Huat Bay, Han-Ming Shen & Choon Nam Ong (2019): Targeted metabolomics reveals differential biological effects of nanoplastics and nanoZnO in human lung cells, *Nanotoxicology*, DOI: [10.1080/17435390.2019.1640913](https://doi.org/10.1080/17435390.2019.1640913)

To link to this article: <https://doi.org/10.1080/17435390.2019.1640913>

 View supplementary material 


 Accepted author version posted online: 05 Jul 2019.
Published online: 24 Jul 2019.

 Submit your article to this journal 

 Article views: 43

 View Crossmark data 

Targeted metabolomics reveals differential biological effects of nanoplastics and nanoZnO in human lung cells

Swee Ling Lim^a, Cheng Teng Ng^b , Li Zou^a, Yonghai Lu^a, Jiaqing Chen^c, Boon Huat Bay^d, Han-Ming Shen^c and Choon Nam Ong^{a,b}

^aSaw Swee Hock School of Public Health, National University of Singapore, Singapore, Singapore; ^bNUS Environmental Research Institute, National University of Singapore, Singapore, Singapore; ^cDepartment of Physiology, Yong Loo Lin School of Medicine, National University of Singapore, Singapore, Singapore; ^dDepartment of Anatomy, Yong Loo Lin School of Medicine, National University of Singapore, Singapore, Singapore

ABSTRACT

Engineered nanomaterials are of public health concern. Recently, there has been an increasing attention on the toxicity of nanoplastics and nanoZnO because of their increasing utilization and presence in the environment. However, knowledge of their toxicological behavior and metabolic interactions with the cellular machinery that determine their potential health effects are extremely limited. In this study, the cellular uptake, cytotoxic effects, and metabolic responses of bronchus epithelial (BEAS-2B) cells exposed to nanopolystyrene (nanoPS) and a widely used metallic nanoparticle, nanoZnO, were investigated using a tandem mass spectrometry-based metabolomics approach. The results revealed that even with low cytotoxicity, these nanoparticles (NPs) affected cell metabolism. NanoPS exposure showed autophagic- and endoplasmic reticulum (ER) stress-related metabolic changes such as increased in amino acids and tricarboxylic acid cycle (TCA) intermediate metabolites, a process known to play a critical role in regulating cell resistance to cytotoxic effects. Both metabolomics profiling and ER-stress pathway, together with quantitative real-time RT-polymerase chain reaction (qRT-PCR) analyses, demonstrated that autophagy was reciprocally regulated to couple metabolic and transcriptional reprogramming. In contrast, nanoZnO-induced ROS-mediated cell death was associated with mitochondrial dysfunction and interference in regulating energy metabolism. Collectively, these two types of NPs were observed to cause perturbations albeit differential in cellular metabolism associated with their cytotoxic effects. Our findings provided an in depth understanding of metabolic changes influenced by two different types of NPs, with contrasting molecular mechanisms for the adverse effects observed.

ARTICLE HISTORY

Received 1 March 2019
Revised 21 May 2019
Accepted 5 June 2019


KEYWORDS


Nanopolystyrene; nanoZnO; lung cells; cytotoxicity; MS/MS-based metabolomics

Introduction

Nanoparticles (NPs) have been reported to pose a threat to the environment and human health. Among them, the occurrence of non-biodegradable nanoplastics is becoming an increasing concern, as nanoplastics recently have been found to accumulate in marine organisms and therefore, could be transferred up the food chain (Bhargava et al. 2018). The reduction in size, due to environmental degradation, could pose a risk to human health, owing to (a) the potential interaction with organic material resulting from their high surface area; (b) difficulty in the removal from the respiratory system due to their polymeric structure and sometimes,

various shapes; and (c) the release of hazardous substances such as persistent organic pollutants (POPs) and plasticizers from their surface (Prata 2018). Therefore, determination of the implications of nanoplastics in human health is an urgent task. Nanopolystyrene (nanoPS) has been shown to internalize efficiently in various cultured cell lines, including rat alveolar epithelial cells (Yacobi et al. 2008), erythrocytes and macrophages (Geiser et al. 2005), and cancer cells (Forte et al. 2016). They were found to be not membrane-bound, and showing potential to interact and damage intracellular structures (Geiser et al. 2005). Moreover, it has been found that nanoPS could affect the growth,

CONTACT Choon Nam Ong  ephocn@nus.edu.sg  Saw Swee Hock School of Public Health, National University of Singapore, 12 Science Drive 2, #11-01, Tahir Foundation Building, Singapore 117549, Singapore

 Supplemental data for this article can be accessed [here](#).

© 2019 Informa UK Limited, trading as Taylor & Francis Group

mortality, changes in feeding activity, reproduction, and abnormal physical formation of the subsequent generation of aquatic organisms (Rosenkranz et al. 2009; Besseling et al. 2014; Nasser and Lynch 2016; Chae and An 2017), in similar ways as many engineered nanomaterials (ENMs) (Lv et al. 2015; Reddy et al. 2016). However, there was evidence that metal particles may trigger additional toxicological pathways making them more toxic than other particle types (e.g. polystyrene) (Lenz et al. 2013). Thus, two nanoparticles, nanoPS and nanoZnO, of different properties, should be investigated in greater detail to compare their toxicological mechanisms. Zinc oxide NP (nanoZnO) has about the third highest global production volume among metal-containing ENMs due to their wide usage in cosmetics, medicine, and as an antibacterial agent and catalyst (Piccinno et al. 2012). Although the toxicity of nanoZnO were studied extensively, the role of reactive oxygen species (ROS) and inflammation were the most common mechanisms being investigated (Vandebriel and De Jong 2012; Chen et al. 2015; Lai et al. 2015). Owing to increasing utilization for both nanoPS and nanoZnO, concerns of their toxicity have also increased. However, knowledge of their toxicological behavior and metabolic interactions with the cellular machinery that determines cell fate is scarce. Both of nanoPS (Prata 2018) and nanoZnO (Monsé et al. 2014) have recently been detected in atmospheric fallout. The respiratory tract is the primary route of exposure to airborne nanoparticles. Hence, the BEAS-2B cell line was selected in this study as it has frequently been acknowledged as a pulmonary cell system suitable for the study of nanoparticles cellular transport and intracellular response (Ekstrand-Hammarström et al. 2012; Gilbert et al. 2012).

Recently, interest in the autophagy process has led to a renewed attention to the interplay between autophagy and cellular metabolism. Protein catabolism was the first defined function for autophagy (Singh and Cuervo 2011). There were two purposes for protein breakdown: to utilize amino acids for cellular fueling and to replenish the intracellular pool of amino acids required to maintain protein synthesis. Furthermore, the tricarboxylic acid cycle (TCA) was expected to become more active during autophagy, as the amino acids generated by the autophagic process were utilized to

sustain energy homeostasis (Rabinowitz and White 2010), leading to modulation of aerobic glycolysis in autophagic cells. More generally, the carbon skeletons of the so-called ketogenic and glucogenic amino acids could be transformed into acetyl-CoA and TCA cycle intermediates, respectively. This explained how autophagy can indirectly fuel the TCA cycle by supplying amino acids (from protein degradation) and thereby contributes to cellular homeostasis. Several nanoparticles showed alteration in amino acids metabolism, which reflected by autophagic protein degradation for recycle and reuse (Saborano et al. 2017). The amino acid could be oxidized in the TCA pathway to produce ATP (Galluzzi et al. 2014). Additionally, earlier nuclear magnetic resonance (NMR) studies suggested that nanoZnO affected the TCA cycle by repressing the enzymes in rat kidney (Yan et al. 2012), rat lung (Lee et al. 2016), and yeast (Babele 2019), resulting in diminished ATP generation and ultimately cell death. With these evidence, it was still unclear how the amino acids and TCA were being affected by nanoparticles to maintain its homeostasis. Therefore, investigation of the potential links of amino acids and TCA in relation to the cell viability was needed to enhance our understanding of the cytotoxicity induced by nanoparticles. In this study, we thus aimed to estimate the changes of amino acids and TCA metabolites induced by nanoZnO and nanoPS using targeted metabolomics strategies. To date, metabolomics still seldom been applied to nanotoxicology, although recent NMR studies have demonstrated the value of using such a platform, for example, gold nanorods (Zhang et al. 2013), silica (Feng et al. 2013), and iron oxide nanoparticles (Feng et al. 2011). In this study, we seek to address this knowledge gap through tandem mass spectrometry-based metabolomics.

To provide a direct evidence of metabolite profile changes caused by NPs and its connection to cell viability, this study used tandem mass spectroscopy coupled with multivariate analyses to investigate the metabolic changes induced by nanoPS and nanoZnO. Our metabolomics-based study integrated two highly sensitive and complementary chromatographic mass spectrometry platforms. With these platforms, we detected significant and dose-dependent changes in the metabolic profiles of human BEAS-2B bronchus epithelial cells that were

treated with nanoPS. Our results revealed that despite slight morphological or viability changes in nanoPS exposure, there was already an increase of various cellular amino acid levels accompanied with increased TCA intermediate metabolites. In contrast, reduced levels of targeted metabolomics profiles accompanied by excessive ROS and mitochondrial damage were observed in nanoZnO-treated lung cells. Our work brought forth a new aspect of nanotoxicity where metabolomics changes were associated with increased nanoPS doses, most likely due to autophagy and oxidative stress, and suggested that nanoPS showed different cytotoxicity mechanisms as compared to nanoZnO.

Materials and methods

Materials

NanoPS (product number G50 from Fisher Scientific, Waltham, MA) and nanoZnO (product number 721077 from Sigma-Aldrich, St. Louis, MO) were prepared in Milli-Q water for hydrodynamic size analysis by dynamic light scattering (DLS). The stock concentration of 1 mg/mL solution was prepared freshly, sonicated, and sterile-filtered.

Chemicals

Methanol, formic acid, and ammonium formate, standards including amino acid standard mixture (AAS18), tryptophan, glutamine, asparagine, citrulline, sodium pyruvate, sodium lactate, fumarate, malic acid, succinic acid, citrate, oxaloacetic acid, α -ketoglutarate, glucose, pyridine, 1-ethyl-3-(3-dimethylaminopropyl) carbodiimide (EDC), 3-nitrophenylhydrazine (hydrochloride) (3-NPH hydrochloride), and isotopically labeled amino acid mix standard (20 amino acids) were purchased from Sigma-Aldrich (St. Louis, MO). $U\text{-}^{13}\text{C}_6\text{-glucose}$ (CLM-481) was obtained from Cambridge Isotope Laboratories (Cambridge, UK). $^{13}\text{C}_6\text{-3-Nitrophenylhydrazine}$ (hydrochloride) ($^{13}\text{C}_6\text{-3NPH}$ hydrochloride) was procured from Cayman Chemical (Ann Arbor, MI). LC-MS grade Acetonitrile was purchased from Merck. Distilled water was purified 'in-house' using a Milli-Q purification system (Bedford, MA).

Characterization of nanoPS

Transmission electron microscopy (TEM) analysis for the nanoPS was performed using the JEOL 1010 TEM. The NanoDrop[®] ND-1000 UV-Vis spectrophotometer (NanoDrop Technologies Inc., Wilmington, DE) was used to analyze the absorption spectrum of nanoPS. In addition, dynamic light scattering (DLS) and zeta potential (Zetasizer Nano ZS, Worcestershire, UK) were measured to assess the hydrodynamic size and surface charge of nanoPS in solution.

Cell culture

Bronchial epithelial BEAS-2B cells was obtained from American Type Culture Collection (ATCC[®] CRL-9609[™]) and grown in Roswell Park Memorial Institute (RPMI 1640) medium (HyClone, Logan, UT), as described in a previous study (Chan et al. 2016). It was supplemented with 1% heat-inactivated fetal bovine serum (FBS, HyClone, Logan, UT), together with 100 $\mu\text{g}/\text{mL}$ streptomycin and 100 units/mL penicillin (PAN-Biotech, Bavaria, Germany). The cells were maintained in an incubator with humidified atmosphere of 37 °C and 5% CO₂.

Cell viability

The cellular viability was measured by the MTS assay (Promega, Vermont, WI), which looked at the reduction of 3-(4,5-dimethylthiazol-2-yl)-5-(3-carboxymethoxyphenyl)-2-(4-sulfophenyl)-2H-tetrazolium (MTS) to formazan in viable cells. Briefly, cells were plated onto 96-well plates. After incubation with the indicated dose of NPs for 24 h at 37 °C, the formazan absorbance was measured at 490 nm. The mean absorbance of non-exposed cells was the reference value for calculating 100% cellular viability.

Transmission electron microscopy (TEM) for cellular uptake and mitochondrion morphology

NPs-treated cells were fixed in 2.5% glutaraldehyde (GA) for 1 h before rinsing three times with phosphate-buffered saline (PBS) at an interval of 5 min each. Samples were osmified with 1% OsO₄ and bits of KFeCN (Agar Scientific Ltd, Stansted, UK) at room temperature for 1 h. Subsequently, samples were dehydrated by immersing in a graded series

of ethyl alcohol for 10 min each and embedded in epoxy resin (polymerization at 60 °C overnight) (Ted Pella Inc., Redding, CA). This was followed by slicing of ultrathin sections, which were then mounted on formvar-coated Cu grids. Sections were stained with lead citrate (BDH, Bristol, UK). Digital micrographs were obtained using a Gatan 792 Bioscan 1 k × 1 k Wide Angle Multiscan charge-coupled device camera attached to the JEOL 1010 TEM (Tokyo, Japan).

ATP colorimetric assay

ATP content was measured in aliquots of mitochondrial suspension by a colorimetric ATP assay kit (AB83355, Abcam, Cambridge, UK) using the phosphorylation of glycerol to generate a quantifiable product at 570 nm. After 24 h, control and treated-cells were collected and treated according to specifications in the manufacturer's instruction manual.

Immunofluorescence assays for reactive oxygen species (ROS) and LC3 autophagy marker

An O₂⁻ sensitive fluorescent dye dihydroethidium (DHE) was used to study the cellular ROS-scavenging activity. Cells were seeded at the concentration of 4 × 10⁵ cells/well on glass coverslips in the 6-well plates for 24 h, before incubation with DHE (D1168, Thermo Fisher Scientific, Waltham, MA) for 30 min in 37 °C. The cells were washed thrice with PBS, followed by fixation with 4% paraformaldehyde for 15 min in room temperature. After washing once with PBS and twice with 1% Triton X-100 in PBS (PBS-TX), the cells were incubated with Cell Mask (C10046, Thermo Fisher Scientific) for 10 min at room temperature. Lastly, the cells were washed thrice with PBS-TX, and mounted onto glass slides in Vectashield with 4',6-diamidino-2-phenylindole (DAPI, Vector Laboratories, Burlingame, CA) before capturing images with a confocal microscope (Olympus Fluoview FV1000 Laser Scanning Confocal Microscopy, Olympus, Tokyo, Japan). The quantification of the intracellular ROS was calculated using *Image J* software analysis (NIH Image J system, Bethesda, MD). It was based on the intensity per cell, with three independent experiments. To study the autophagy, intracellular localization of microtubule-associated protein 1 light chain 3 (LC3) was

evaluated by confocal microscopy using an anti-LC3 antibody (L7543, Sigma-Aldrich, St. Louis, MO). Autophagy inhibitor chloroquine (CQ, C6628-25G, Sigma-Aldrich, St. Louis, MO) was added onto the cells for 4 hours before NPs treatment. After 24 h treatment of NPs, the cells were fixed in 4% paraformaldehyde and blocked with 1% BSA for 1 h. This was followed by overnight incubation with LC3. After washing, the cells were labeled with a secondary anti-rabbit antibody (Sigma-Aldrich, St. Louis, MO) for 1 h and with DAPI. Finally, the cells were covered with a coverslip, and examined with a confocal microscope.

Western blot for LC3 autophagy marker

Whole cell lysates were extracted using a mixture of radio-immunoprecipitation (RIPA) lysis buffer (Pierce, Waltham, MA), Halt Protease and Phosphatase Inhibitor Cocktail (Pierce, Waltham, MA), and 0.5 ethylenediaminetetraacetic acid (EDTA) (Pierce, Waltham, MA) on ice for 15 min. After cell lysis, the lysates were centrifuged for 15 min at 15,000 rpm, 4 °C. Protein concentration was determined using the microtiter Bio-Rad Protein Assay (Bio-Rad, Hercules, CA). The same amount of protein lysates was denatured at 95 °C in 5× loading dye for 5 min and loaded into each well of the 10% sodium dodecyl sulfate-polyacrylamide gel. After separation by electrophoresis, proteins were transferred to a polyvinylidene difluoride (PVDF) membrane using a semi-dry system (Bio-Rad, Hercules, CA). Transfer of proteins was carried out at 20 V for 1 h. Blocking of the PVDF membrane was subsequently done using 5% skim milk, followed by incubation with primary antibodies that included anti-LC3 (1:3000 dilution) (L7543, Sigma-Aldrich, St. Louis, MO), and anti-GAPDH (1:1000 dilution) (SC-32233, Santa Cruz Biotechnology, Santa Cruz, TX) at 4 °C overnight. Subsequently, incubation with the HRP-conjugated secondary antibody (Sigma-Aldrich, St. Louis, MO) was carried out for 1 h at room temperature. The SuperSignal West Pico Chemiluminescent ECL substrate (Pierce, Waltham, MA) was used to detect the protein bands which were then quantified using the GS-800 densitometer (Bio-Rad, Hercules, CA).

RNA extraction, reverse transcription (RT), and quantitative real-time RT-polymerase chain reaction (qRT-PCR) for endoplasmic reticulum (ER) stress primer

The Purelink RNA Mini Kit (Catalog number: 12183018A, Thermo Fisher Scientific, Waltham, MA) was used to isolate total RNA. RNA quality was assessed using the NanoDrop ND-1000 spectrophotometer at the absorbance reading of 260 and 280 nm wavelengths. BEAS-2B cells were lysed, followed by the addition of an equal volume of 70% ethanol. Samples were then transferred into a Spin Column and centrifuged for 15 s at 13,200 rpm. After which, the samples were subjected to washing, using the buffers provided inside the kit and spun dry to remove excessive ethanol, followed by elution with RNase-free water. For cDNA conversion, Agilent AffinityScript qPCR cDNA synthesis kit (Genomax Technologies, Madison, WI) was used according to manufacturer's instructions. cDNA was stored at -20°C for later use. A mixture consisting diluted cDNA, SYBR Green PCR Master Mix (Thermo Fisher Scientific, Waltham, MA) and primer for each gene was analyzed by a 7900HT Fast Real-Time PCR machine (Thermo Fisher Scientific, Waltham, MA) following the thermal profile settings: 95°C , 20 s; 95°C , 1 s followed by 60°C , 20 s for 40 cycles. Each sample was run in triplicates and GAPDH was used as the housekeeping gene for normalization. Alterations in gene expression were expressed as fold change using the $2^{-\Delta\Delta\text{CT}}$ method.

MS/MS-based metabolomics analyses

Isotope-labeled internal standard mixture preparation

The suspension of isotopically labeled amino acid mix standard was added in $10\ \mu\text{L}$ of hydroxyl chloride (1 N) and $440\ \mu\text{L}$ of distilled water. The $500\ \mu\text{L}$ of dissolved isotopically labeled amino acid mix standard was then diluted 10 times by distilled water and mixed with $^{13}\text{C}_6$ -glucose as an internal standard for amino acids and glucose quantification. A mixture of eight organic acids (lactate, malic acid, succinic acid, fumarate, citrate, pyruvate, oxaloacetic acid, and α -ketoglutarate) was derivatized by 200 mM of $^{13}\text{C}_6$ -3-NPH and 120 mM of EDC-6% pyridine solution at 40°C for 1 h. After derivatization,

the solution was diluted 20 times by methanol/water (4/1) mixture solution as internal standard mixture (Han et al. 2013) for organic acids quantification. This solution was stored at -20°C .

Sample preparation

Freeze-dried cell pallets were treated with $100\ \mu\text{L}$ isotopically labeled amino acids/glucose internal standard and $400\ \mu\text{L}$ cold methanol. After homogenization by TissueLyser LT (Qiagen, Valencia, CA) for 10 min at 25 Hz, the homogenized solutions were sonicated for 10 min in icy-cold water. The mixtures were centrifuged for 20 min in 14,000 rpm at 5°C . The supernatant was aliquot into three portions. One portion ($100\ \mu\text{L}$), was dried using 99.9% nitrogen and reconstituted in $500\ \mu\text{L}$ acetonitrile/water (90:10, v/v) before analysis, and used for quantitative analyses of amino acids. Another portion ($100\ \mu\text{L}$), was spiked with $^{13}\text{C}_6$ -3-NPH-labeled internal standards before analysis, and used for quantitative analyses of 3-NPH derivatized organic acids (Han et al. 2013). The last portion ($100\ \mu\text{L}$) was treated through a two-step derivatization method (Lu et al. 2017), and isolated for quantitative analyses of glucose. Quality control (QC) was performed by spiking certain amount of native and labeled standards into a pooled methanol extract of cells, and eight QCs were analyzed along with the samples to ensure the reliability of the method and the instrument stability.

LC-MS/MS analysis

The quantitative analyses of amino acids and bio-organic compounds were performed by an Agilent 1200 HPLC system coupled to a 6410 Triple Quadrupole (QQQ) mass spectrometer (Agilent Technologies, Santa Clara, CA) equipped with an electrospray ionization source. Amino acids were analyzed in positive ion mode, whereas eight 3-NPH derivatized organic acids were detected in negative ion mode. The mass spectrum was acquired in the multiple reaction monitoring (MRM) mode with a capillary voltage of 3500 V on positive mode as well as 4500 V on negative mode, a gas temperature of 350°C , a gas flow of 12 L/min, and the nebulizer nitrogen gas flow rate of 30 psi. The retention time, MRM transition, fragmentor voltage, and collision energy (CE) are shown in Supplemental Table S1.

Amino acids were separated by using an Acquity UPLC BEH Amide column (2.1 mm × 100 mm, 1.7 μm, Waters, Milford, MA). The mobile phases A (30% acetonitrile with 0.1% formic acid and 10 mmol/L ammonium formate) and B (95% acetonitrile with 0.1% formic acid and 10 mmol/L ammonium formate) were employed. The gradient program was set as the following: 0–1 min, 100% B; 1–3 min, 100–92% B; 3–9 min, 92–85% B; 9–9.5 min, 85–80% B; 9.5–10.5 min, 80% B; 10.5–12 min, 80–70% B; 12–15 min, 70–15% B; 15–19 min, 15% B; 19–19.5 min, 15–100% B. The flow rate was set at 0.5 mL/min. The column temperature and injection volume were set at 40 °C and 5 μL, respectively. Eight 3-NPH derivatized organic acids were separated by using an Acquity UPLC BEH C18 column (2.1 mm × 100 mm, 1.7 μm, Waters, Milford, MA). The mobile phases A (5% acetonitrile in water with 0.01% formic acid) and B (acetonitrile with 0.01% formic acid) were employed. The gradient program was the following: 0–1 min, 10% B; 1–3 min, 10–50% B; 3–5 min, 50–60% B; 5–8.5 min, 60% B; 8.5–10 min, 60–100% B; 10–16 min, 100% B. The flow rate was set at 0.4 mL/min. The column temperature and the injection volume were set at 40 °C and 5 μL, respectively.

GC-MS/MS analysis

The quantitative analysis of glucose was performed by an Agilent 7890 GC system coupled to a 7000B QQQ mass detector (Agilent Technologies, Palo Alto, CA) equipped with a chemical ionization (CI) source. A J&W HP-5MS-23 column (60 m × 0.25 mm × 0.25 μm, USA) was used for sample separation. The injection volume was 1 μL in pulsed splitless mode. The flow rate of the carrier gas, helium, was 2 mL/min. The GC oven temperature was started at 120 °C for 1 min and raised to 200 °C at 25 °C/min, then raised to 217 °C at 1.5 °C/min, and eventually raised to 300 °C at 25 °C/min, and maintained at 300 °C for 5 min. Mass spectrum was acquired in positive MRM mode with parameters: methane as reactant gas, and gas flow was set at 20%, ion source temperature was at 250 °C. The optimized parameters on MRM transition and CE are summarized in [Supplemental Table S1](#).

Statistical analysis

Data were presented as the mean ± standard error of mean (SEM) for three independent experiments. Statistical analyses were performed using SPSS statistical software program 25 (SPSS, Chicago, IL). Data were analyzed by one-way analysis of variance (ANOVA) followed by the Tukey's test for comparison between control and treatment groups. Statistical significance was set at $p < 0.05$.

Results and discussion

Characterization and cellular uptake of NPs

The detailed physicochemical characteristics of NPs are presented in [Figure 1\(A–C\)](#), indicating that nanoPS and nanoZnO formed a stable suspension in aqueous media. We first confirmed the uptake of NPs into BEAS-2B cells by performing transmission electron microscopy (TEM) as shown in [Figure 1\(D\)](#). Both nanoPS and nanoZnO were detected in the cytoplasm of the cells in the form of electron dense clusters, which were found to be enclosed by vesicles. Based on the potential for uptake, it could be anticipated that inhaled NPs would reach the deep parts of the lung and cross the lung epithelial lining as observed by Wright and Kelly (2017). However, we noted that the nanoPS presented lower cytotoxicity as compared to nanoZnO ([Figure 1\(C\)](#)). NanoPS treatment affected the cell viability significantly only at >10 μg/ml after 24 h, whereas nanoZnO caused dramatic decrease at >5 μg/ml. NanoPS decreased cell viability of bronchus epithelial cells in a dose-dependent manner, which may be correlated with the amount of internalization of nanoPS. Based on these results, 10 μg/ml of nanoZnO and two different doses of nanoPS (10 and 50 μg/ml, herein refer as low dose (nanoPS_LD) and high dose (nanoPS_HD) of nanoPS, respectively) were selected for the subsequent study. We considered this concentration because it was a dose that started to trigger cell death. It, thus, allowed the analysis of the main metabolic changes in the viable, but probably damaged, remaining cells.

Cytotoxicity response of NPs

We determined cellular oxidative damage using the DHE assay for ROS measurement. Our findings

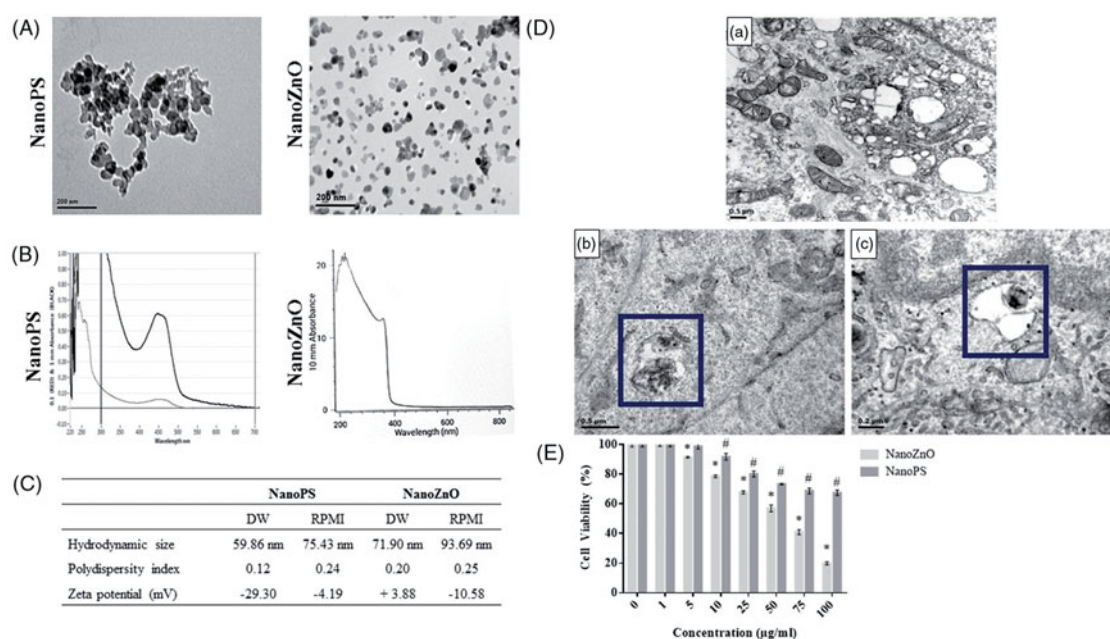


Figure 1. Characterization of nanoparticles (NPs) and their cellular uptake. (A) TEM micrographs. (B) UV-vis of nanoPS revealed an absorption peak at 450 nm, whereas the nanoZnO showed two absorption peaks at 220 nm, and 360 nm. (C) Size distribution and zeta potential from DLS. (D) TEM micrograph of untreated and NPs-treated cells. Uptake of nanoparticles were indicated inside the cell vacuole (boxed area). (a) control; (b) nanoZnO; (c) nanoPS. (E) MTS assay showed a dose-dependent significantly decreased in cell viability caused by nanoPS and nanoZnO after 24 h. The results were the mean \pm SEM of three independent experiments. Symbols (*, #) represented the significantly different ($p < 0.05$) as compared with the control. [DLS: dynamic light scattering; DW: deionized water; RPMI: Roswell Park Memorial Institute; UV-vis: ultraviolet-visible]

showed significantly higher ROS levels in the cells exposed to nanoZnO than in the nanoPS (Figure 2(A)). The generation of ROS was significantly enhanced by 633.1%, 193.6%, and 344.2% after 24 h of treatment with nanoZnO, nanoPS_LD, and nanoPS_HD, respectively, as compared to control (Figure 2(B)). Mitochondria are considered to be a major source of ROS that affect cellular energy metabolism. We next examined whether the NPs affected mitochondrial function. As shown in Figure 2(C), swollen mitochondria was observed clearly in nanoZnO, indicating a disruption in integrity of the mitochondria. In nanoZnO-treated cells, the mitochondria area (Supplemental Figure S1) was significantly increased ($0.98 \pm 0.05 \mu\text{m}^2$), as compared with untreated cells ($0.47 \pm 0.02 \mu\text{m}^2$). In contrast, there was no alteration of mitochondrial morphology observed in nanoPS treatment. The effect of nanoZnO on the mitochondrial membrane potential of BEAS-2B cells was further evaluated using the JC-1 (5,6,6'-tetrachloro-1,1',3,3'-tetraethylbenzimidazolylcarbocyanine iodide) kit (Supplementary materials and methods). Our results showed that nanoZnO

exhibited a significantly increased in JC-1 monomers than control, suggesting that nanoZnO caused the loss of mitochondrial potential in bronchus epithelial cells (Supplemental Figure S2). The cytotoxic effects of nanoZnO could be based on a mechanism of particle dissolution and zinc ion (Zn^{2+}) release. Accordingly, the high levels of Zn^{2+} could have been a direct result of mitochondrial permeability transition pore opening and cytochrome c releasing, ultimately leading to apoptosis (Xia et al. 2006). Mitochondrial damage induced by nanoZnO allowed the release of free radicals from mitochondria into the cytoplasm, thus explained the relatively higher ROS in nanoZnO than nanoPS-treated cells (Figure 2(B)). Since the cellular adenosine triphosphate (ATP) level is another important characteristic for evaluating the function of mitochondria, and, as shown in Figure 2(D), nanoZnO significantly decreased the relative cellular ATP levels by approximately 50%. Meanwhile, nanoPS indicated only slight change in the cellular ATP levels (Figure 2(D)). Collectively, nanoZnO-induced ROS-mediated cell death in pulmonary epithelial cells

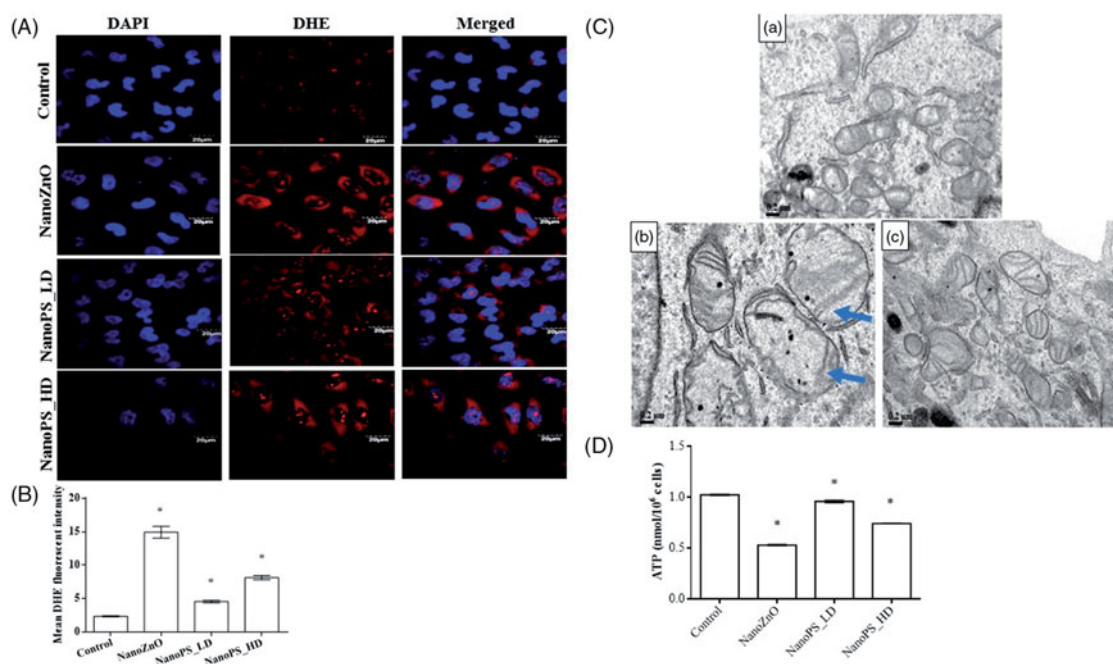


Figure 2. Cytotoxicity effects of NPs. (A) The ROS was determined by DHE fluorescence and quantitative evaluation of mean DHE fluorescence intensity was performed (B). (C) To reveal mitochondria morphology influenced by NPs, TEM analysis was conducted. An abnormal shape of mitochondrion (arrow) was evident in cells treated with nanoZnO. (a) control; (b) nanoZnO; (c) nanoPS. (D) Effect of NPs on cellular ATP levels. The results were the mean \pm SEM of three independent experiments. Symbol (*) represented $p < 0.05$ as compared to control.

was caused by the collapse of mitochondrial membrane permeabilization (MMP) and the corresponding decreased in the relative cellular ATP level.

Accumulating evidence suggested that ROS directly or indirectly affects endoplasmic reticulum (ER) homeostasis and protein folding (Malhotra and Kaufman 2007). Upon stress, the misfolded proteins accumulated in the ER and the unfolded proteins translocated to the cytosol, to be degraded by the proteasome. The ER attempted to remove these proteins by activating unfolded protein response (UPR) system that constituted series of functions initiated by stress transducers like eukaryotic translation initiation factor 2- α kinase 3 (EIF2AK3), endoplasmic reticulum to nucleus signaling 1 (ERN1), and activating transcription factor 6 (ATF6). When this exceeded the UPR clearance capacity, the cell utilized autophagy to degrade these accumulated misfolded or unfolded proteins (Marquez and Xu 2012). In this study, we observed that nanoPS activated ER stress even at low cytotoxic level (Figure 3(A)), suggesting that autophagy was a more susceptible index for nanoPS. We also found dose-dependently significant increase in the expression of ATF6, DDIT3, and ERN1 in the cells treated

with nanoPS, as compared with the control (Figure 3(A)). A simplified illustration demonstrating the influence of nanoPS on mechanism of autophagy induced by ER stress is shown in Figure 3(B). In addition, elevation of ER stress markers (DDIT3 and ERN1) is also shown in nanoZnO-treated cells (Figure 3(A)), which could result in apoptosis, through the expression of the apoptotic genes BCL2L11/BIM/BBC3/PUMA, and MAP3K5/ASK1/TRAF2 (Christen, Camenzind, and Fent 2014).

Further, nanoPS induced autophagosomes accumulation and promoted LC3-II in a dose-dependent manner (Figure 3(C,D)). LC3-II is located in autophagosomes and essential for maturation of autophagosomes. It is commonly regarded as the autophagic marker. Based on the results on confocal microscopy, there were few LC3-II puncta in the control and nanoZnO groups, but they were obvious in both nanoPS_LD and nanoPS_HD groups after 24 h (Figure 3(C)). To further verify the results, we performed western blotting and found the expression levels of the LC3-II proteins increased with nanoPS treatment in a dose-dependent manner (Figure 3(D)). Previous study has reported that the lysosomal accumulation of nanoPS caused

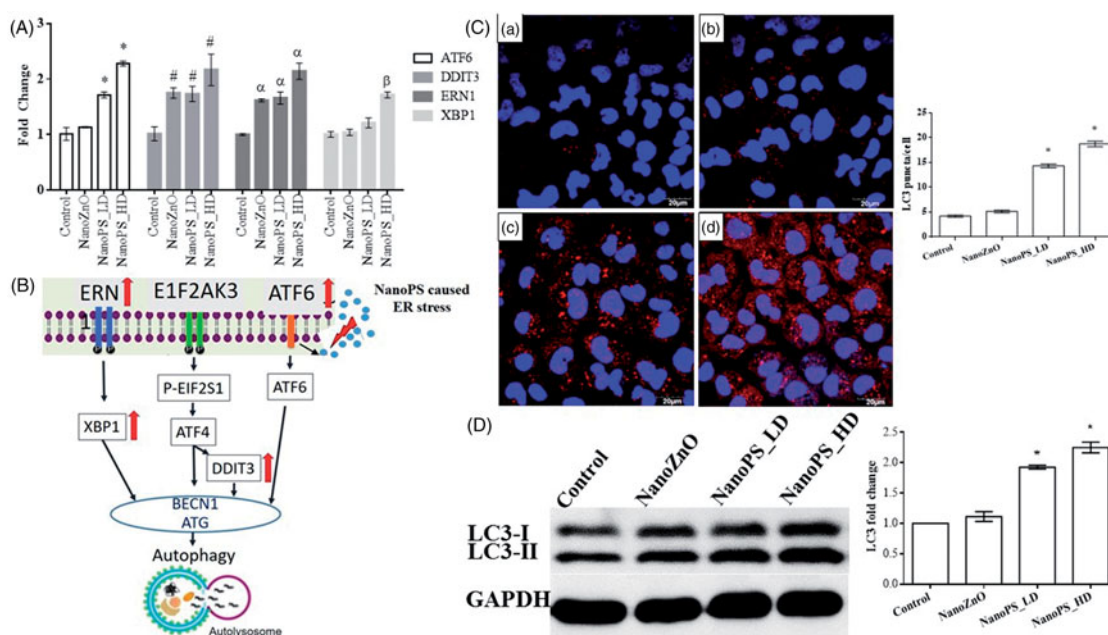


Figure 3. NanoPS-induced ER stress-mediated autophagy. (A) Quantitative real-time RT-polymerase chain reaction (qRT-PCR) analysis showed an increasing trend in the expression of ER stress-related genes in nanoPS. The results were the mean \pm SEM of three independent experiments. Symbols (*, #, α , β) represented the significantly different ($p < 0.05$) as compared with the control. [ATF6: activating transcription factor 6; DDI3: DNA damage-inducible transcript 3 protein; ERN1: Endoplasmic Reticulum to Nucleus Signaling 1; XBP1: X-box binding protein 1]. (B) A simplified illustration demonstrated the effect of nanoPS on mechanism of autophagy induced by ER stress. (C, left) Immunofluorescence assay of microtubule-associated protein 1 light chain 3 (LC3) a marker of autophagosomes. (Red: LC3; Blue: nucleus. Scale bar, 20 μ m). The cells were pretreated with autophagy inhibitor chloroquine (CQ) for 4 h before nanoPS treatment for 24 hours. It revealed that nanoPS treatment increased the number of LC3 fluorescence puncta (red), but not in nanoZnO. (a) control; (b) nanoZnO; (c) nanoPS_LD; (d) nanoPS_HD. LC3 puncta per cell were quantified by ImageJ analysis from three independent experiments, which based on the intensity per cell. The data represented as LC3 puncta/cell of each group compared with control (C, right) Symbol (*) represented $p < 0.05$ as compared to control. (D, left) We further determined LC3 using Western blotting analysis. GAPDH served as a loading control. (D, right) Bar graph showed the relative fold change of LC3 (normalized to GAPDH). The results were the mean \pm SEM of three independent experiments. Symbols (*, #) represented the significantly different ($p < 0.05$) as compared with the control. Please refer to the color version of this figure online.

induction of the autophagic response through activation of transcription factor EB (TFEB), which manifested as an increase in lysosome–autophagosome fusion and, ultimately, enhanced clearance of autophagic cargo (Song et al. 2015). Again, the levels of LC3-II did not change when the cells were exposed to nanoZnO (Figure 3(D)). To determine whether nanoPS-induced ER stress contributed directly to autophagy, we treated BEAS-2B cells with the chemical chaperone tauroursodeoxycholic acid (TUDCA), which is known to selectively inhibit ER stress (Yu et al. 2015). The lung cells were treated with TUDCA (1 mM) for 2 h before exposure to nanoPS. The results indicated that TUDCA treatment decreased nanoPS-induced autophagy (Supplemental Figure S3). Taken together, our data demonstrated that nanoPS induced autophagy through the ER stress caused by misfolded protein aggregation in bronchus epithelial cells.

Targeted metabolic profiles in NPs-treated cells

In this study, two inter-related analytical platforms were used to measure the metabolites changes induced by nanoPS and nanoZnO, including liquid chromatography-tandem mass spectrometry with positive ionization (LC-MS/MS+), liquid chromatography-tandem mass spectrometry with negative ionization (LC-MS/MS-), and gas chromatography mass spectrometry (GC-MS) (with positive ionization via electron impact ionization). Of these, 27 metabolites were readily detectable in the NPs-treated cells (Supplemental Table S2). Importantly, the QC samples (Figure 4(A)) were clustered close together suggesting that the MS/MS analysis method was reliable. The changes of targeted metabolites were demonstrated in the heat-maps (Figure 4(B)). We noticed a trend where cellular amino acids were down-regulated in nanoZnO and, on the contrary,

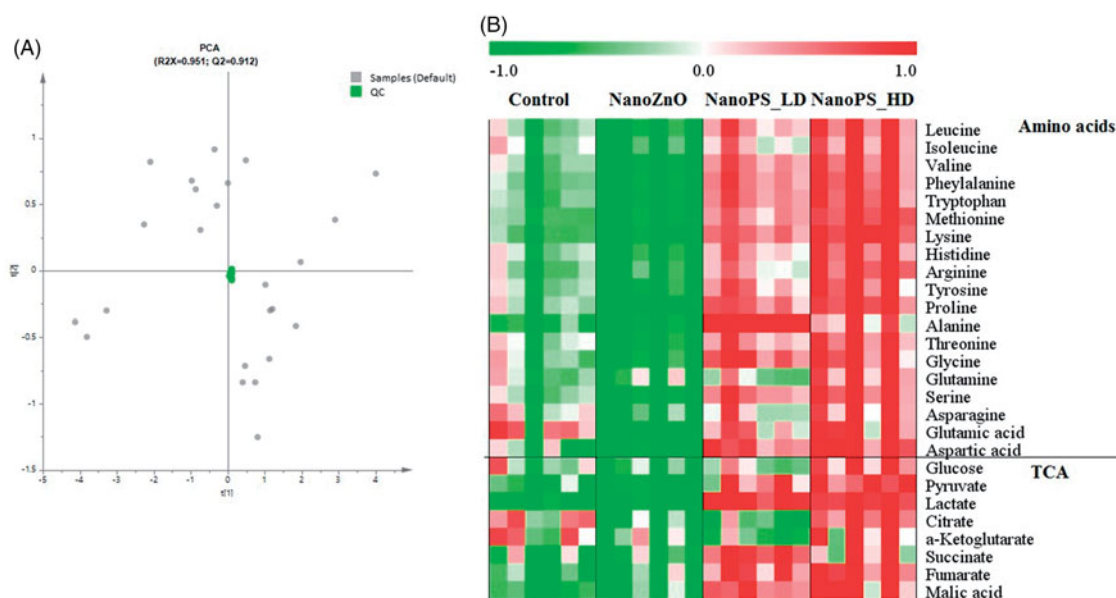


Figure 4. Metabolite profile differences between control and NPs-treated cells. The six replicates samples were analyzed in a random order, and pooled quality control (QC) samples were inserted into the analysis sequence to evaluate the stability of mass spectrometry analytical system. (A) The QC samples were clustered together in the principal component analysis (PCA) scores plots. (B) Heat-map of amino acids and tricarboxylic acid cycle (TCA) metabolites in NPs-treated cells compared to untreated cells. The metabolic profiles of the NPs-treated cells demonstrated apparent metabolic differences, which indicated the nanoZnO and nanoPS induced specific alterations in their metabolism.

these metabolites tend to up-regulate with increasing doses of nanoPS.

Metabolic changes in NPs

After normalization with cell counts (Supplemental Table S3), we observed that the metabolic shifts following treatment of low dose nanoPS were apparently different from those treated with similar dose of nanoZnO, and a trend in dose-response based on multivariate analysis was shown for nanoPS exposure (Figure 5(A)). Compared to the non-treated cells, NanoPS_LD tend to have higher levels of amino acids (phenylalanine, tryptophan, methionine, lysine, proline, alanine, glycine, serine, and aspartic acid), carbohydrate (pyruvate and lactate), and TCA intermediates metabolites (succinate, fumarate, and malic acid), in order to maintain their cell viability, and against the cytotoxicity effects. As observed in this study, most metabolic changes induced by nanoPS exposures were associated with autophagy, anti-oxidative protection, and perturbed energetic metabolism. The results were consistent with previous findings that autophagy provided cells with amino acids, which could be oxidized in the TCA to produce ATP (Galluzzi et al. 2014).

Amino acids are essential metabolic intermediates involved in the process of molecule biosynthesis, energy generation and are required for cell growth, proliferation and differentiation. The levels of intracellular amino acids are kept even by the balance of their inflow, utilization, including the synthesis of proteins or as metabolic intermediates, and recycling. Nevertheless, the fine balance between amino acid availability and autophagic activity affected the cell death susceptibility (Loos et al. 2013). The marked induction of amino acids in the whole-cell lysate of nanoPS (Figure 5(A)) supported the possibility that autophagy could lead to a localized high amino acids concentration in the lysosome, and also degraded protein when autophagy was activated, in order to regulate the cell viability. Furthermore, significantly elevated levels of amino acids are also likely due to stress hormones being produced in nanoPS.

Interestingly, based on the up-regulation of pyruvate and lactate in the nanoPS (Figure 5(A)), we suggested that nanoPS-treated cells being less reliant on aerobic glycolysis, sustaining cellular homeostasis by utilizing autophagic degradation products to fuel cell metabolism, as supported by previous study (Rabinowitz and White 2010). In brief, in

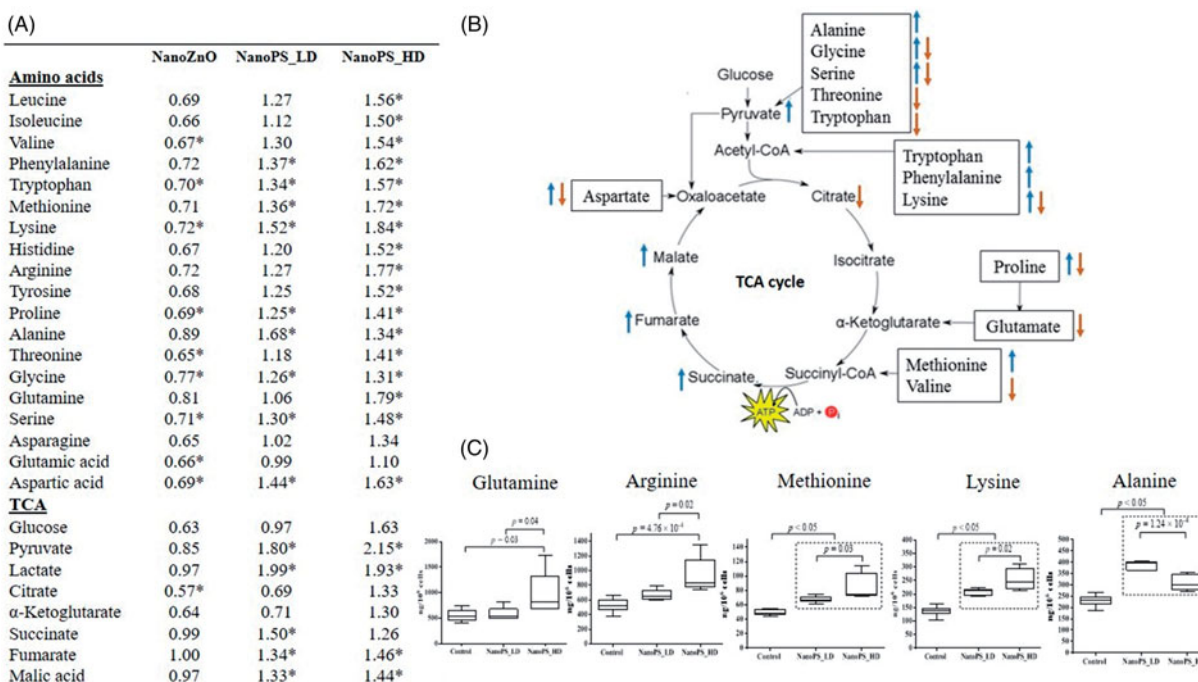


Figure 5. Quantitative results of NPs in metabolomics analyses. (A) Table indicated the influence of NPs on amino acids and TCA-related metabolites. The numbers were the ratio of the treated mean divided by the control mean. Symbol (*) represented the $p < 0.05$ as compared with the control. (B) A summary of relevant metabolic responses of BEAS-2B cells to nanoZnO and nanoPS_LD exposure. Arrow in orange or blue represent a significant increase or decrease in the nanoZnO or nanoPS_LD, respectively, as compared with the non-treated groups. (C) The box plots showed relative quantification of 5 amino acids, including methionine, lysine, arginine, alanine, and glutamine, which were dose-dependently significant increase in nanoPS as compared with control. Please refer to the color version of this figure online.

aerobic metabolism, glucose is converted into pyruvate, and generates large amount of ATP via the TCA cycle, electron transport chain and oxidative phosphorylation. Moreover, in order to maintain a high glycolytic flux, lactate has to be transported out of the cells according to its concentration gradient (Zhang et al. 2008). In fact, pyruvate is also interchangeable with alanine or malate by single reactions, catalyzed by alanine aminotransferase (ALT) or malic enzyme, respectively, in both the cytosol and mitochondria (Corbet and Feron 2017). We, therefore, noticed significant elevation of alanine, serine, and threonine, tryptophan, and malic acids levels in nanoPS-treated cells (Figure 5(A)), which were directly related to pyruvate as an intermediate in their metabolism. Other studies have also shown that pulmonary inflammation induced by silica dust could result in a shift to anaerobic metabolic pathway in the lung, as indicated by an increased level of lactate (Hu et al. 2008). Hence, we believed that nanoPS might interfered the energy metabolism and converted glucose into

lactate or alanine in the lung cells in order to supply enough energy for regular homeostasis.

Meanwhile, nanoZnO demonstrated differences in the metabolic shift pattern. A significantly ($p < 0.05$) decrease in the levels of amino acids (valine, tryptophan, lysine, proline, threonine, glycine, serine, glutamic acid, and aspartic acid) and TCA intermediate metabolites (citrate) were observed in the cells treated with nanoZnO (Figure 5(A)), thus, suggesting that nanoZnO may cause a perturbation in cellular energy metabolism. It was known that excessive proteolysis was detrimental to cell survival. The decreased levels of intracellular amino acid in nanoZnO caused the unsustainability of TCA cycle for survival, which consistent to our viability results (Figure 1C). Similar to our TCA (citrate) result in nanoZnO (Figure 5(A)), the intragastric administration of nanoZnO on rat kidney suggested that nanoZnO were dissolved as Zn^{2+} and inhibited the enzymes of TCA cycle, resulting in decreased levels of citrate, succinate and α -ketoglutarate (Yan et al. 2012). In consistent with nanosilica study (Feng

et al. 2013), the stress-related metabolic variations included the decreased of alanine, glycine, tryptophan, valine, and ATP were also found in nanoZnO. Based on a previous NMR metabolomics study (Lee et al. 2016), the decreasing level of glycine might be used to replenish the consumed glutathione. A summary of relevant significant ($p < 0.05$) metabolic responses of BEAS-2B cells to nanoZnO and nanoPS_LD exposure is illustrated in Figure 5(B). We related the NPs-induced cytotoxicity effects with amino acids and energy metabolism, and found the corresponding changes in metabolite profiles could be associated with their cell viability.

Additionally, high-dose exposures of nanoPS resulted in elevated levels of an even larger range of the amino acids and TCA intermediate metabolites (Figure 5(A)), indicating that nanoPS might induced the uptake of exogenous amino acids, thus, contributing to the increased concentration of intracellular free amino acids. There were similarities in the trend but significant differences ($p < 0.05$) in the response of the dose-dependent nanoPS-treated cells, as compared to the normal cells, characterized by increased of glutamine, arginine, methionine, and lysine (Figure 5(C)). This suggested that the stimulation of a higher dose of nanoPS nanoparticles led to enhanced autophagy and stress-response including catabolism of carbohydrate and protein (derived from intermediates of TCA cycle and amino acids), and oxidative stress-response (derived from ADP). However, due to a significant finding in reduction of alanine in high doses exposure, as compared with low dose of nanoPS (Figure 5(C)), a possible explanation for the abovementioned finding might be due to the downregulation of alanine caused by synthesis of more coenzyme A (CoA). CoA was acetylated to form acetyl-CoA, which was not only one of the central substrates for anabolic metabolism but also the important product of multiple catabolic circuits (Martinez et al. 2014).

Based on our metabolomics studies, one of the most prominent differences between the nanoPS and nanoZnO exposure was the significant elevation in the levels of glutamine, methionine, and glycine in nanoPS-treated cells, but depleted in nanoZnO cells (Figure 5(A)). These amino acids are precursors of glutathione (GSH) and play important roles in maintaining optimal intracellular redox

environments for the proper function of cellular proteins (Wu et al. 2004; Green and Lamming 2019). Obvious elevations in the levels of precursors of GSH implied that de novo GSH synthesis was activated in nanoPS-treated cells, particularly in high dose of nanoPS, which was not the case for nanoZnO (Figure 5(A)). Hence, we suggested that the anti-oxidant capability of nanoPS was stronger than that of the nanoZnO, and in consistent with their cell viability results. Furthermore, it was interesting to note that among all the non-essential amino acids (NEAAs), glutamine displayed the increment in abundance which preceded others in high dose of nanoPS (Figure 5(C)), presumably in a vain attempted to restore other NEAAs. It was recognized that glutamine is an important carrier for shuttling of nitrogen among tissues due to its capacity to readily donate amide and amino nitrogen (Tan, Sim, and Long 2017). Therefore, as shown in our results (Figure 5(A)), glutamine tends to restore the levels of TCA cycle intermediates downstream of α -KG (succinate, fumarate, and malate) and many cell lines used this pathway to supply the bulk of carbon flux through the TCA cycle (Lin et al. 2012). After entering the cell, glutamine was converted to glutamate, then entered the TCA cycle and this resulted in the production of ATP via oxidative phosphorylation (Lin et al. 2012). Although our current data failed to differentiate the contribution by glutamine from autophagy or extracellular nutrition to maintaining cellular homeostasis, it seemed likely that autophagy was the main mechanism for providing glutamine needed to fuel the oxidative mitochondrial metabolism under nanoPS exposure.

Moreover, in arginine and proline metabolism pathway, arginine is synthesized from citrulline by the continuous action of cytosolic enzymes (argininosuccinate synthetase/argininosuccinate lyase). Under the action of arginases, arginine is converted into urea and ornithine. Ornithine is transported into the mitochondria through the mitochondrial inner membrane and participates in the synthesis of citrulline to complete the ornithine cycle (Tapiero et al. 2002). Increased arginine levels (Figure 5(C)) in our study was supported by nanoTiO₂ study, which demonstrated similar trend in arginine accompanying with decreased urea and ornithine (Tucci et al. 2013). Lower activity of urea and ornithine cycle led to reduce polyamine synthesis, which then might

signify reduced proliferation. Thus, this could partly explain the cytotoxic effect of nanoPS.

Collectively, metabolism regulates autophagy, and autophagy has a profound impact on metabolism. In our study, autophagy was observed in the lung cells in response to oxidative stress generated as a consequence of exposure to nanoPS. Therefore, the increment of amino acid and TCA-related metabolites induced by nanoPS might have been due to degraded protein when autophagy was activated (Onodera and Ohsumi 2005). However, when the energetic requirements of the autophagic process itself are taken into consideration, the final energy balance would be rather poor if energy were only to be obtained from the amino acids generated from protein breakdown. The perturbed energy metabolism (less reliant on aerobic glycolysis) was also shown in nanoPS treatment, i.e. increased in pyruvate and lactate, which led to less net energy. Moreover, the autophagic machinery itself requires ATP levels to be sufficient for initiation and progression, and also the need for ATP to maintain lysosomal pH (Arias and Cuervo 2011). Hence, the higher the autophagic activity, the higher is the ATP cost to maintain elevated levels of autophagic flux (Loos et al. 2013). This might be one explanation why the nanoPS treatment has led to net loss in ATP.

On the other hand, NanoZnO demonstrated the enhancement in ROS activity, causing alteration in amino acid metabolism and tricarboxylic acid cycle, and reduction in ATP generation. Indeed, improper function of autophagic tend to cause the accumulation of malfunctioning mitochondria and redox active protein aggregates that, in the long term, have widespread metabolic consequences, including a reduction in mitochondrial ATP synthesis and an increased generation of genotoxic ROS (Galluzzi et al. 2014). This observation thus supported our findings that nanoZnO showed negligible effect in autophagy.

Conclusion

In summary, MS/MS-based metabolomics revealed the differential effects of nanoPS and nanoZnO on BEAS-2B human epithelia lung cells. NanoPS was associated with the activation of autophagy and interference of energy metabolism. Whereas the

nanoZnO was related with overproduction of ROS, mitochondrion depolarization, and inability to sustain the amino acids metabolisms and TCA for survival. Our study provided a novel insight into the regulation mechanisms of ROS-autophagy-mitochondria-metabolism axis, which could contribute to a better understanding of the toxicity of different NPs. Investigation of the metabolic effects on the respiratory cells can be helpful in understanding the specific metabolic responses in target organs. It could not be certain that all the literature reviewed here reflected real environment or *in vivo* conditions, but these studies indicated valuable directions for future work and mitigated the relevant debatable issues. Therefore, future studies should further investigate the mechanism underlying acute and chronic nanoPS and nanoZnO toxicity, especially in *in vivo* or human subjects.

Acknowledgements

The authors thank Associate Professor David Tai Leong from the Department of Chemical and Biomolecular Engineering, National University of Singapore for dynamic light scattering (DLS) analyses.

Disclosure statement

No potential conflict of interest was reported by the authors.

Funding

This study was supported by funding from the Center for Environmental and Occupational Health, Saw Swee Hock School of Public Health, National University of Singapore [R-608-000-007-731] and the NUS Environmental Research Institute (NERI) Secondment Fund to OCN [R-706-000-005-133].

ORCID

Cheng Teng Ng  <http://orcid.org/0000-0002-4002-1725>

References

- Arias, E., and A. M. Cuervo. 2011. "Chaperone-Mediated Autophagy in Protein Quality Control." *Current Opinion in Cell Biology* 23(2): 184–189. doi:10.1016/j.ceb.2010.10.009.
- Babele, P. K. 2019. "Zinc Oxide Nanoparticles Impose Metabolic Toxicity by de-Regulating Proteome and Metabolome in *Saccharomyces cerevisiae*." *Toxicology Reports* 6: 64–73. doi:10.1016/j.toxrep.2018.12.001.

- Besseling, E., B. Wang, M. Lüring, and A. A. Koelmans. 2014. "Nanoplastic Affects Growth of *S. obliquus* and Reproduction of *D. magna*." *Environmental Science & Technology* 48(20): 12336–12343. doi:10.1021/es503001d.
- Bhargava, S., S. S. C. Lee, L. S. M. Ying, M. L. Neo, S. L. M. Teo, and S. Valiyaveetil. 2018. "Fate of Nanoplastics in Marine Larvae: A Case Study Using Barnacles, *Amphibalanus amphitrite*." *ACS Sustainable Chemistry & Engineering* 6(5): 6932–6940. doi:10.1021/acssuschemeng.8b00766.
- Chae, Y., and Y. J. An. 2017. "Effects of Micro- and Nanoplastics on Aquatic Ecosystems: Current Research Trends and Perspectives." *Marine Pollution Bulletin* 124(2): 624–632. doi:10.1016/j.marpolbul.2017.01.070.
- Chan, T. K., X. Y. Loh, H. Y. Peh, W. N. F. Tan, W. S. D. Tan, N. Li, I. J. J. Tay, W. S. F. Wong, and B. P. Engelward. 2016. "House Dust Mite-Induced Asthma Causes Oxidative Damage and DNA Double-Strand Breaks in the Lungs." *Journal of Allergy and Clinical Immunology* 138(1): 84–96. doi:10.1016/j.jaci.2016.02.017.
- Chen, J. K., C. C. Ho, H. Chang, J. F. Lin, C. S. Yang, M. H. Tsai, H. T. Tsai, and P. Lin. 2015. "Particulate Nature of Inhaled Zinc Oxide Nanoparticles Determines Systemic Effects and Mechanisms of Pulmonary Inflammation in Mice." *Nanotoxicology* 9(1): 43–53. doi:10.3109/17435390.2014.886740.
- Christen, V., M. Camenzind, and K. Fent. 2014. "Silica Nanoparticles Induce Endoplasmic Reticulum Stress Response, Oxidative Stress and Activate the Mitogen-Activated Protein Kinase (MAPK) Signaling Pathway." *Toxicology Reports* 1: 1143–1151. doi:10.1016/j.toxrep.2014.10.023.
- Corbet, C., and O. Feron. 2017. "Cancer Cell Metabolism and Mitochondria: Nutrient Plasticity for TCA Cycle Fueling." *Biochimica et Biophysica Acta (BBA) – Reviews on Cancer* 1868(1): 7–15. doi:10.1016/j.bbcan.2017.01.002.
- Ekstrand-Hammarström, B., C. M. Akfur, P. O. Andersson, C. Lejon, L. Österlund, and A. Bucht. 2012. "Human Primary Bronchial Epithelial Cells Respond Differently to Titanium Dioxide Nanoparticles than the Lung Epithelial Cell Lines A549 and BEAS-2B." *Nanotoxicology* 6(6): 623–634. doi:10.3109/17435390.2011.598245.
- Feng, J., J. Li, H. Wu, and Z. Chen. 2013. "Metabolic Responses of HeLa Cells to Silica Nanoparticles by NMR-Based Metabolomic Analyses." *Metabolomics* 9(4): 874–886. doi:10.1007/s11306-013-0499-8.
- Feng, J., H. Liu, K. K. Bhakoo, L. Lu, and Z. Chen. 2011. "A Metabonomic Analysis of Organ Specific Response to USPIO Administration." *Biomaterials* 32(27): 6558–6569. doi:10.1016/j.biomaterials.2011.05.035.
- Forté, M., G. Iachetta, M. Tussellino, R. Carotenuto, M. Prisco, M. De Falco, V. Laforgia, and S. Valiante. 2016. "Polystyrene Nanoparticles Internalization in Human Gastric Adenocarcinoma Cells." *Toxicology in Vitro* 31: 126–136. doi:10.1016/j.tiv.2015.11.006.
- Galluzzi, L., F. Pietrocola, B. Levine, and G. Kroemer. 2014. "Metabolic Control of Autophagy." *Cell* 159(6): 1263–1276. doi:10.1016/j.cell.2014.11.006.
- Geiser, M., B. Rothen-Rutishauser, N. Kapp, S. Schürch, W. Kreyling, H. Schulz, M. Semmler, V. I. Hof, J. Heyder, and P. Gehr. 2005. "Ultrafine Particles Cross Cellular Membranes by Nonphagocytic Mechanisms in Lungs and in Cultured Cells." *Environmental Health Perspectives* 113(11): 1555–1560. doi:10.1289/ehp.8006.
- Gilbert, B., S. C. Fakra, T. Xia, S. Pokhrel, L. Mädler, and A. E. Nel. 2012. "The Fate of ZnO Nanoparticles Administered to Human Bronchial Epithelial Cells." *ACS Nano* 6(6): 4921–4930. doi:10.1021/nn300425a.
- Green, C. L., and D. W. Lamming. 2019. "Regulation of Metabolic Health by Essential Dietary Amino Acids." *Mechanisms of Ageing and Development* 177: 186–200. doi:10.1016/j.mad.2018.07.004.
- Han, J., S. Gagnon, T. Eckle, and C. H. Borchers. 2013. "Metabolomic Analysis of Key Central Carbon Metabolism Carboxylic Acids as Their 3-Nitrophenylhydrazones by UPLC/ESI-MS." *Electrophoresis* 34(19): 2891–2900. doi:10.1002/elps.201200601.
- Hu, J. Z., D. N. Rommereim, K. R. Minard, A. Woodstock, B. J. Harrer, R. A. Wind, R. P. Phipps, and P. J. Sime. 2008. "Metabolomics in Lung Inflammation: A High-Resolution (1)h NMR Study of Mice Exposed to Silica Dust." *Toxicology Mechanisms and Methods* 18(5): 385–398. doi:10.1080/15376510701611032.
- Lai, X., Y. Wei, H. Zhao, S. Chen, X. Bu, F. Lu, D. Qu, L. Yao, J. Zheng, and J. Zhang. 2015. "The Effect of Fe₂O₃ and ZnO Nanoparticles on Cytotoxicity and Glucose Metabolism in Lung Epithelial Cells." *Journal of Applied Toxicology* 35(6): 651–664. doi:10.1002/jat.3128.
- Lee, S. H., T. Y. Wang, J. H. Hong, T. J. Cheng, and C. Y. Lin. 2016. "NMR-Based Metabolomics to Determine Acute Inhalation Effects of Nano- and Fine-Sized ZnO Particles in the Rat Lung." *Nanotoxicology* 10(7): 924–934. doi:10.3109/17435390.2016.1144825.
- Lenz, A. G., E. Karg, E. Brendel, H. Hinze-Heyn, K. L. Maier, O. Eickelberg, T. Stoeger, and O. Schmid. 2013. "Inflammatory and Oxidative Stress Responses of an Alveolar Epithelial Cell Line to Airborne Zinc Oxide Nanoparticles at the Air-Liquid Interface: A Comparison with Conventional, Submerged Cell-Culture Conditions." *BioMed Research International* 2013: 652632. doi:10.1155/2013/652632.
- Lin, T. C., Chen, Y. R. E. Kensicki, A. Y. J. Li, M. Kong, Y. Li, R. P. Mohny, H. M., et al. 2012. "Autophagy: Resetting Glutamine-Dependent Metabolism and Oxygen Consumption." *Autophagy* 8(10): 1477–1493. doi:10.4161/auto.21228.
- Loos, B., A. M. Engelbrecht, R. A. Lockshin, D. J. Klionsky, and Z. Zakeri. 2013. "The Variability of Autophagy and Cell Death Susceptibility: Unanswered Questions." *Autophagy* 9(9): 1270–1285. doi:10.4161/auto.25560.
- Lu, Y., L. Zou, J. Su, E. S. Tai, C. Whitton, R. M. van Dam, and C. N. Ong. 2017. "Meat and Seafood Consumption in

- Relation to Plasma Metabolic Profiles in a Chinese Population: A Combined Untargeted and Targeted Metabolomics Study." *Nutrients* 9(7): 683. doi:10.3390/nu9070683.
- Lv, J., S. Zhang, L. Luo, J. Zhang, K. Yang, and P. Christie. 2015. "Accumulation, Speciation and Uptake Pathway of ZnO Nanoparticles in Maize." *Environmental Science: Nano* 2: 68–77. doi:10.1039/C4EN00064A.
- Malhotra, J. D., and R. J. Kaufman. 2007. "Endoplasmic Reticulum Stress and Oxidative Stress: A Vicious Cycle or a Double-Edged Sword?" *Antioxidants & Redox Signaling* 9(12): 2277–2293. doi:10.1089/ars.2007.1782.
- Marquez, R. T., and L. Xu. 2012. "BCL2: Beclin 1 Complex: Multiple Mechanisms Regulating Autophagy/Apoptosis Toggle Switch." *American Journal of Cancer Research* 2(2): 214–221.
- Martinez, D. L., Y. Tsuchiya, and I. Gout. 2014. "Coenzyme a Biosynthetic Machinery in Mammalian Cells." *Biochemical Society Transactions* 42(4): 1112–1117. doi:10.1042/BST20140124.
- Monsé, C., C. Monz, D. Dahmann, C. Asbach, B. Stahlmecke, N. Lichtenstein, K. E. Buchwald, R. Merget, J. Bünger, and T. Brüning. 2014. "Development and Evaluation of a Nanoparticle Generator for Human Inhalation Studies with Airborne Zinc Oxide." *Aerosol Science and Technology* 48(4): 418–426. doi:10.1080/02786826.2014.883064.
- Nasser, F., and I. Lynch. 2016. "Secreted Protein Eco-Corona Mediates Uptake and Impacts of Polystyrene Nanoparticles on *Daphnia Magna*." *Journal of Proteomics* 137: 45–51. doi:10.1016/j.jprot.2015.09.005.
- Onodera, J., and Y. Ohsumi. 2005. "Autophagy Is Required for Maintenance of Amino Acid Levels and Protein Synthesis under Nitrogen Starvation." *Journal of Biological Chemistry* 280(36): 31582–31586. doi:10.1074/jbc.M506736200.
- Piccinno, F., F. Gottschalk, S. Seeger, and B. Nowack. 2012. "Industrial Production Quantities and Uses of Ten Engineered Nanomaterials in Europe and the World." *Journal of Nanoparticle Research* 14(9): 1109. doi:10.1007/s11051-012-1109-9.
- Prata, J. C. 2018. "Airborne Microplastics: Consequences to Human Health?" *Environmental Pollution* 234: 115–126. doi:10.1016/j.envpol.2017.11.043.
- Rabinowitz, J. D., and E. White. 2010. "Autophagy and Metabolism." *Science* 330(6009): 1344–1348. doi:10.1126/science.1193497.
- Reddy, P. V. L., J. A. Hernandez-Viezas, J. R. Peralta-Videa, and J. L. Gardea-Torresdey. 2016. "Lessons Learned: Are Engineered Nanomaterials Toxic to Terrestrial Plants?" *Science of the Total Environment* 568: 470–479. doi:10.1016/j.scitotenv.2016.06.042.
- Rosenkranz, P., Q. Chaudhry, V. Stone, and T. F. Fernandes. 2009. "A Comparison of Nanoparticle and Fine Particle Uptake by *Daphnia Magna*." *Environmental Toxicology and Chemistry* 28(10): 2142–2149. doi:10.1897/08-559.1.
- Saborano, R., T. Wongpinyochit, J. D. Totten, B. F. Johnston, F. P. Seib, and I. F. Duarte. 2017. "Metabolic Reprogramming of Macrophages Exposed to Silk, Poly(Lactic-co-Glycolic Acid), and Silica Nanoparticles." *Advanced Healthcare Materials* 6(14): 1601240. doi:10.1002/adhm.201601240.
- Singh, R., and A. M. Cuervo. 2011. "Autophagy in the Cellular Energetic Balance." *Cell Metabolism* 13(5): 495–504. doi:10.1016/j.cmet.2011.04.004.
- Song, W., L. Popp, J. Yang, A. Kumar, V. S. Gangoli, and L. Segatori. 2015. "The Autophagic Response to Polystyrene Nanoparticles Is Mediated by Transcription Factor EB and Depends on Surface Charge." *Journal of Nanobiotechnology* 13(1): 87. doi:10.1186/s12951-015-0149-6.
- Tan, H. W. S., A. Y. L. Sim, and Y. C. Long. 2017. "Glutamine Metabolism Regulates Autophagy-Dependent mTORC1 Reactivation during Amino Acid Starvation." *Nature Communications* 8(1): 338. doi:10.1038/s41467-017-00369-y.
- Tapiero, H., G. Mathé, P. Couvreur, and K. Tew. 2002. "l-Arginine." *Biomedicine & Pharmacotherapy* 56(9): 439–445. doi:10.1016/S0753-3322(02)00284-6.
- Tucci, P., G. Porta, M. Agostini, D. Dinsdale, I. Iavicoli, K. Cain, A. Finazzi-Agró, G. Melino, and A. Willis. 2013. "Metabolic Effects of TiO₂ Nanoparticles, a Common Component of Sunscreens and Cosmetics, on Human Keratinocytes." *Cell Death & Disease* 4: e549. doi:10.1038/cddis.2013.76.
- Vandebriel, R. J., and W. H. De Jong. 2012. "A Review of Mammalian Toxicity of ZnO Nanoparticles." *Nanotechnology, Science and Applications* 5: 61–71. doi:10.2147/NSA.S23932.
- Wright, S. L., and F. J. Kelly. 2017. "Plastic and Human Health: A Micro Issue?" *Environmental Science & Technology* 51(12): 6634–6647. doi:10.1021/acs.est.7b00423.
- Wu, G., Y. Z. Fang, S. Yang, J. R. Lupton, and N. D. Turner. 2004. "Glutathione Metabolism and Its Implications for Health." *The Journal of Nutrition* 134(3): 489–492. doi:10.1093/jn/134.3.489.
- Xia, T., M. Kovochich, J. Brant, M. Hotze, J. Sempf, T. Oberley, C. Sioutas, J. I. Yeh, M. R. Wiesner, and A. E. Nel. 2006. "Comparison of the Abilities of Ambient and Manufactured Nanoparticles to Induce Cellular Toxicity according to an Oxidative Stress Paradigm." *Nano Letters* 6(8): 1794–1807. doi:10.1021/nl061025k.
- Yacobi, N. R., L. Maio, J. Xie, S. F. Hamm-Alvarez, Z. Borok, K. J. Kim, and E. D. Crandall. 2008. "Polystyrene Nanoparticles Trafficking across Alveolar Epithelium." *Nanomedicine: Nanotechnology, Biology and Medicine* 4(2): 139–145. doi:10.1016/j.nano.2008.02.002.
- Yan, G., Y. Huang, Q. Bu, L. Lv, P. Deng, Y. Wang, Y. Yang, Q. Liu, X. Cen, and Y. Zhao. 2012. "Zinc Oxide Nanoparticles Cause Nephrotoxicity and Kidney Metabolism Alterations in Rats." *Journal of Environmental Science and Health, Part A. Toxic/Hazardous Substances and Environmental Engineering* 47(4): 577–588. doi:10.1080/10934529.2012.650576.
- Yu, K. N., S. H. Chang, S. J. Park, J. Lim, J. Lee, T. J. Yoon, J. S. Kim, and M. H. Cho. 2015. "Titanium Dioxide Nanoparticles Induce Endoplasmic Reticulum Stress-Mediated Autophagic Cell Death via Mitochondria-

- Associated Endoplasmic Reticulum Membrane Disruption in Normal Lung Cells." *PLoS One* 10(6): e0131208. doi:[10.1371/journal.pone.0131208](https://doi.org/10.1371/journal.pone.0131208).
- Zhang, L., L. Wang, Y. Hu, Z. Liu, Y. Tian, X. Wu, Y. Zhao, H. Tang, C. Chen, and Y. Wang. 2013. "Selective Metabolic Effects of Gold Nanorods on Normal and Cancer Cells and Their Application in Anticancer Drug Screening." *Biomaterials* 34(29): 7117–7126. doi:[10.1016/j.biomaterials.2013.05.043](https://doi.org/10.1016/j.biomaterials.2013.05.043).
- Zhang, S., G. A. N. Gowda, V. Asiago, N. Shanaiah, C. Barbas, and D. Raftery. 2008. "Correlative and Quantitative ¹H NMR-Based Metabolomics Reveals Specific Metabolic Pathway Disturbances in Diabetic Rats." *Analytical Biochemistry* 383(1): 76–84. doi:[10.1016/j.ab.2008.07.041](https://doi.org/10.1016/j.ab.2008.07.041).